DESIGN AND DEVELOPMENT OF SOFT X-RAY LASER

AVCO EVERETT RESEARCH LABORATORY, INC.
EVERETT, MASSACHUSETTS

DECEMBER 1976

DESIGN AND DEVELOPMENT OF SOFT X-RAY LASER

SEMI-ANNUAL TECHNICAL REPORT

AVCO EVERETT RESEARCH LABORATORY, INC.
a Subsidiary of Avco Corporation
Everett, Massachusetts 02149

December 1976

Contract No. N00173-76-C-0214

supported by

DEFENSE ADVANCED RESEARCH PROJECTS AGENCY
ARPA Order No. 2694

monitored by

NAVAL RESEARCH LABORATORY
Washington, D.C. 20375

FOREWORD

ARPA Order No: 2694

Program Code No: 421

Name of Contractor: AERL, Inc.

Effective Date of Contract: 22 March 1976

Contract Expiration Date: 22 Dec. 1976

Amount of Contract: $363,711

Contract No: N00173-76-C-0214

Principal Investigator: Dr. H. W. Friedman
(617) 389-3000, Ext. 473

Scientific Officer: Dr. R. Elton, Code 5520
(202) 767-2754

Short Title of Work: Soft X-Ray Laser

ABSTRACT

Progress in the theoretical and experimental effort of the soft x-ray laser work is outlined. The lithium vapor model has been refined to include the effects of autoionization and the stimulated Raman gain of the laser system has been correctly calculated. A single short pulse from the mode locked train of CO_2 pulses has been isolated and is ready to be injected into the "Big Bang" laser for amplification. The experimental chamber, vacuum system and focusing optics is complete and the grazing incidence spectrometer is assembled. A dye laser system tuned to 9584Å has been built and tested.

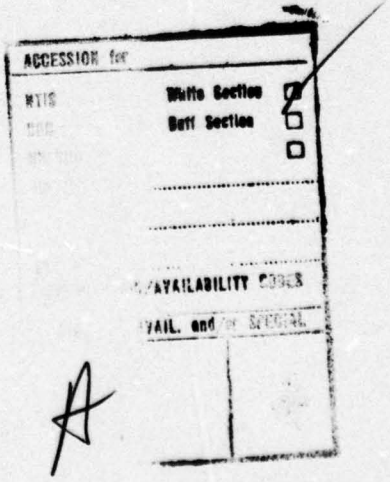

UNCLASSIFIED

SECURITY CLASSIFICATION OF THIS PAGE (When Data Entered)

REPORT DOCUMENTATION PAGE		READ INSTRUCTIONS BEFORE COMPLETING FORM
1. REPORT NUMBER	2. GOVT ACCESSION NO.	3. RECIPIENT'S CATALOG NUMBER
4. TITLE (and Subtitle) Design and Development of Soft X-Ray Laser		5. TYPE OF REPORT & PERIOD COVERED Semi-Annual Technical Rpt, March - December 1976 6. PERFORMING ORG. REPORT NUMBER
7. AUTHOR(s) Dr. H. W. Friedman		8. CONTRACT OR GRANT NUMBER(s) N00173-76-C-0214
9. PERFORMING ORGANIZATION NAME AND ADDRESS Avco Everett Research Laboratory, Inc. 2385 Revere Beach Parkway Everett, Massachusetts 02149		10. PROGRAM ELEMENT, PROJECT, TASK AREA & WORK UNIT NUMBERS N/A
11. CONTROLLING OFFICE NAME AND ADDRESS Defense Advanced Research Projects Agency ARPA Order No. 2694		12. REPORT DATE December 1976 13. NUMBER OF PAGES 58
14. MONITORING AGENCY NAME & ADDRESS(if different from Controlling Office) Naval Research Laboratory Washington, D. C. 20375		15. SECURITY CLASS. (of this report) Unclassified 15a. DECLASSIFICATION/DOWNGRADING SCHEDULE

16. DISTRIBUTION STATEMENT (of this Report)

Approved for public release; distribution unlimited.

17. DISTRIBUTION STATEMENT (of the abstract entered in Block 20, if different from Report)

18. SUPPLEMENTARY NOTES

19. KEY WORDS (Continue on reverse side if necessary and identify by block number)

Laser
X-ray
Optical Pumping
Stimulated Raman

20. ABSTRACT (Continue on reverse side if necessary and identify by block number)

Progress in the theoretical and experimental effort of the soft x-ray laser work is outlined. The lithium vapor model has been refined to include the effects of autoionization and the stimulated Raman gain of the laser system has been correctly calculated. A single order pulse from the mode locked train of CO_2 pulses has been isolated and is ready to be injected into the "Big Bang" laser for amplification. The experimental chamber, a vacuum system and focusing optics is complete and the grazing incidence spectrom-

DD FORM 1 JAN 73 1473 EDITION OF 1 NOV 65 IS OBSOLETE

UNCLASSIFIED

SECURITY CLASSIFICATION OF THIS PAGE (When Data Entered)

(20)
eter is assembled. A dye laser system tuned to 9584 Å has been built and tested.

TABLE OF CONTENTS

LIST OF ILLUSTRATIONS

I. INTRODUCTION

The Soft X-ray Laser Program at AERL involves several tasks, both theoretical and experimental. The progress of these tasks during the first six months of this contract will be documented in this report and the plans for the final three months of the contract presented.

The primary emphasis of the theoretical effort is to model the laser kinetics of the lithium vapor system in a more careful manner. We have already shown that the gain of the lithium vapor laser is larger than that predicted by the standard gain formula. The correct process which describes the gain is a stimulated Raman Anti-Stokes interaction and the appropriate gain calculation has been carried out. In addition several new processes including auto-ionizing photoabsorptive transitions have been incorporated into the laser kinetic model and the implications of these processes have been investigated in both a laboratory demonstration as well as in large scale devices.

The experimental program for this Phase I effort involves the investigation of the basic kinetic processes which are necessary for the successful demonstration of the soft x-ray laser. A CO_2 laser system is to be assembled capable of delivering sufficient short pulse energy to heat a thin metallic target foil to a blackbody radiator of the order of 50 eV. The emission from the radiation source is to be analyzed to verify the spectral distribution necessary for effective optical pumping of the lithium vapor system. A dye laser is also to be built and tuned to the required

resonance transition necessary for stimulated Raman action in the singly ionized lithium manifold. Finally, using the dye laser as a diagnostic probe, a lithium vapor optically excited by the CO_2 laser produced plasma will be investigated as to its metastable state population and induced soft x-ray fluorescence.

II. THEORETICAL WORK

The theoretical effort in the areas of the Raman gain calculation and the effect of auto-ionizing collisions are presented in the two papers included as an appendix to this progress report.

III. DYE LASER SYSTEM

A dye laser system tuned to the 9584Å resonance transition of the singly ionized lithium state is required. Recently, a family of near infrared emitting dyes, carbocyanines, has been investigated and lasing has been achieved in the 8000Å - 1100Å regime using both flashlamp and ruby laser pumping sources. The flashlamp pumped configuration suffers from high dye degradation and poor window seals on the dye cell. In addition, the ever-present possibility of flashlamp explosion is rendered more hazardous because the carcinogenic IR dye is in close proximity to the lamp structure. The ruby laser pump, on the other hand, does not have these problems since the UV fluorescence can be easily filtered from the red output and the ruby laser can be well separated from the IR dye cell. However, the expense of a Q-switched ruby laser, ~20K, is not insignificant.

An alternate pump source is a coaxial dye laser using a red emitting dye such as one of the Rhodamine group. The pulse energy of such lasers is comparable to the ruby but the pulse duration is a factor of 10 larger and therefore the peak power is a factor of 10 lower. Since one of the most important parameters for a dye laser pump is peak power, it is not obvious at the outset that the coaxial dye laser will successfully pump the IR cell to lasing. However, the low cost and availability of coaxial dye lasers render this approach very attractive and, indeed, this is the method we have chosen. Figure 1 shows a schematic layout of the coaxial laser pumped IR dye laser. The inner diameter of the coaxial dye cell is 1 cm and the active

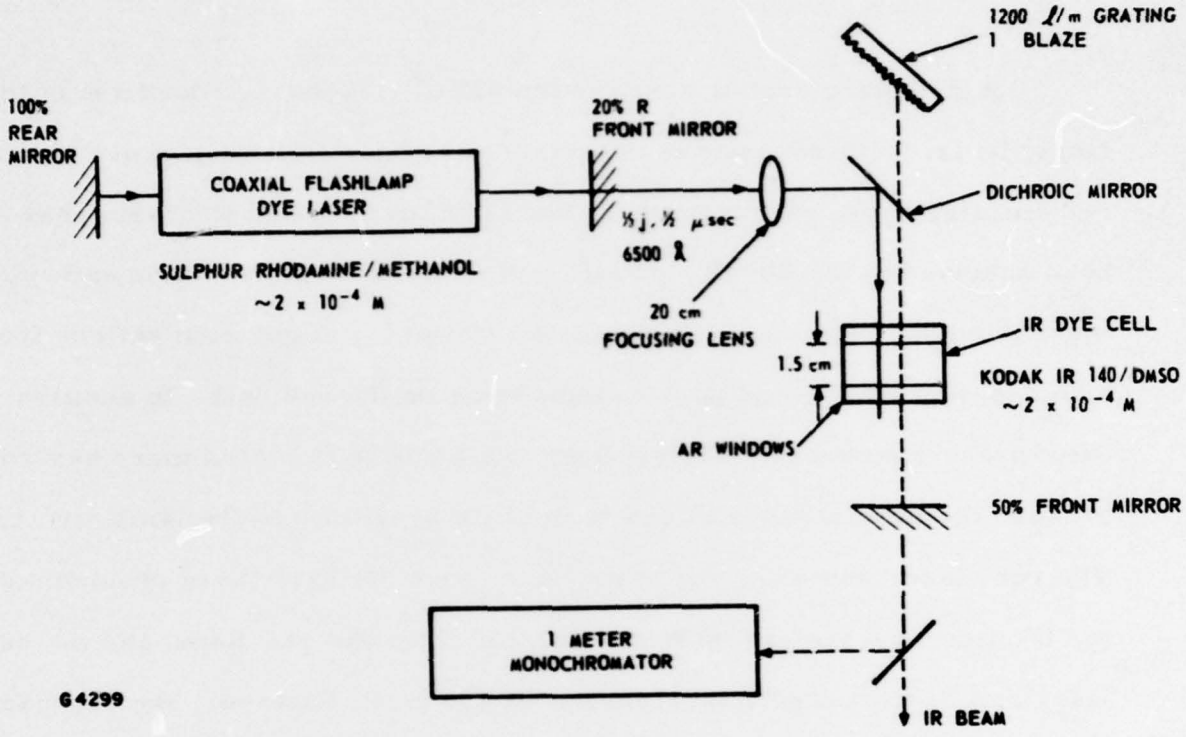

Fig. 1 Schematic Layout of the IR Dye Laser

gain length is 10 cm. The driving capacitor stores a maximum of 100j at 24KV and the entire electrical system has a risetime of about 10^{-7} sec. Using a solution of 3×10^{-4}M of sulforhodamine 101 in methonal, the output energy is 0.62j with a pulse width of ~ 1/2 μsec and beam divergence of ~ 40 milliradians. The large beam divergence of the coaxial laser is a result of the stable, multimode cavity consisting of a maximum reflection rear mirror with a 3 meter radius of curvature and a 20% reflection flat output mirror.

With no wavelength tuning in the optical cavity and broadband mirrors, the spectral characteristics of the coaxial laser was a center wavelength of ~ 6840Å and a bandwidth of ~ 200Å. As far as a spectral match is concerned, the coaxial dye laser with sulforhodamine at 6840 is close to the ruby laser at 6943 and it is expected that the extinction length in the infrared dye is similar. The main difference between the coaxial laser pump and the ruby laser is peak power.

The coaxial laser output is focused into the infrared dye cell by means of a glass lens whose focal length is 15 cm giving a spot size of ~ 3 mm. Therefore the pump intensity in the dye cell is ~ 20 MW/cm^2. The pump light is combined along the optic axis of the dye cell by means of a dichroic mirror as shown in Fig. 1.

The infrared dye cell itself is constructed out of stainless steel with quartz windows which are sealed using teflon o-rings. The infrared dye is flowed transverse to the optic axis by a small pump and a .5μ filter located between the pump and the cell removes photodecomposition particulates and alleviates the "seed" bubble problem. The only materials

in the IR dye system including the pump and motor are 316 stainless steel, quartz and teflon. The entire IR dye system is modularized for quick removal to a proper disposal facility. Such precautions are advisable because the dye, Kodak 940, is carcinogenous and the solvent DMSO is not only incompatible with most plastics and common metals but also freely penetrates skin, thereby transporting the dye directly into the body.

Wavelength tuning of the IR dye cell is accomplished by means of diffraction grating which replaces the conventional rear mirror of the optical cavity. The grating is ruled at 1200 ℓ/mm and blazed for 1μ in the first order. A tuning curve as a function of dye concentration is shown in Fig. 2. It is seen that a concentration of $\sim 5 \times 10^{-5}$ M adequately covers the 9584Å line.

A photomultiplier measurement of the 1/2 power bandwidth indicates approximately 10Å bandwidth. The bandwidth can be lowered by a factor of 3-5 using a telescope to expand the IR beam thereby increasing the effective grating area. A telescope, made commercially for nearby YAG (1.06μ) has been purchased and will soon be installed and tested.

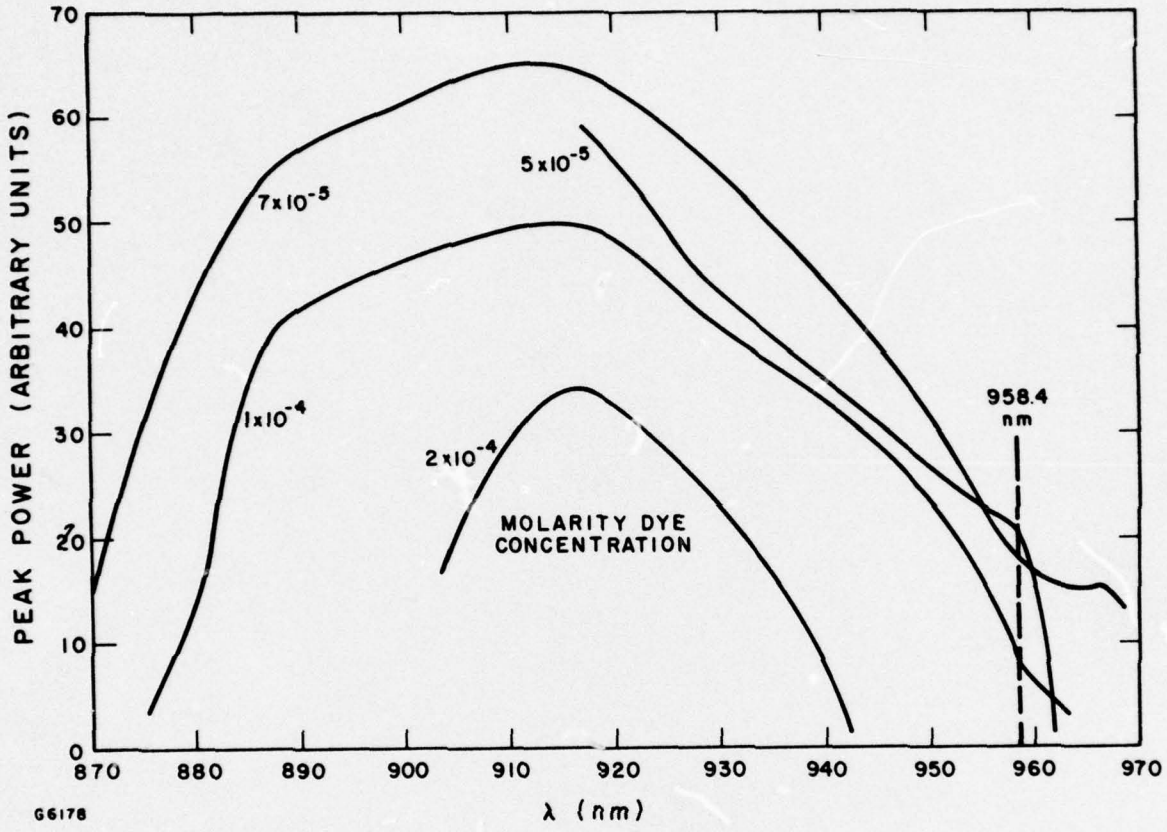

Fig. 2 Tuning Curve for Dye Kodak IR 140

IV. CO_2 LASER SYSTEM

A large CO_2 laser system has been built and is presently undergoing test. The goal of this phase of the experimental effort is to generate a 50 joule pulse of approximately 2 nsec duration. The pulse will be used to irradiate a thin foil target which, in turn, will emit incoherent pumping radiation.

A block diagram of the CO_2 laser system is shown in Fig. 3. The oscillator emits a short pulse of CO_2 radiation of about 10-20 mJ with a duration of ~2nsec and a beam diameter of ~1cm. This pulse is expanded by means of an off axis, aspheric mirror system to a diameter of ~20 cm and passed through a large laser amplifier commonly referred to at AERL as "Big Bang".

The detailed optical system used to generate the 2nsec pulse from the oscillator is shown schematically in Fig. 4. The optical cavity is formed by a 10m radius of curvature rear copper mirror and an uncoated salt flat. The mode locking element, a Brewster angle germanium crystal with a lithium niobate transducer is inside the cavity. The transducer is driven at twice the inverse of the round trip cavity time which for the nominal 250 cm cavity is 30 MHz. In actual practice, the resonant frequency is adjusted according to precise crystal resonances, R. F. equipment resonances and thermal effects, and the cavity length is then adjusted repositioning the position of the salt flat. A trace of the mode locked pulse train is shown in Fig. 5.

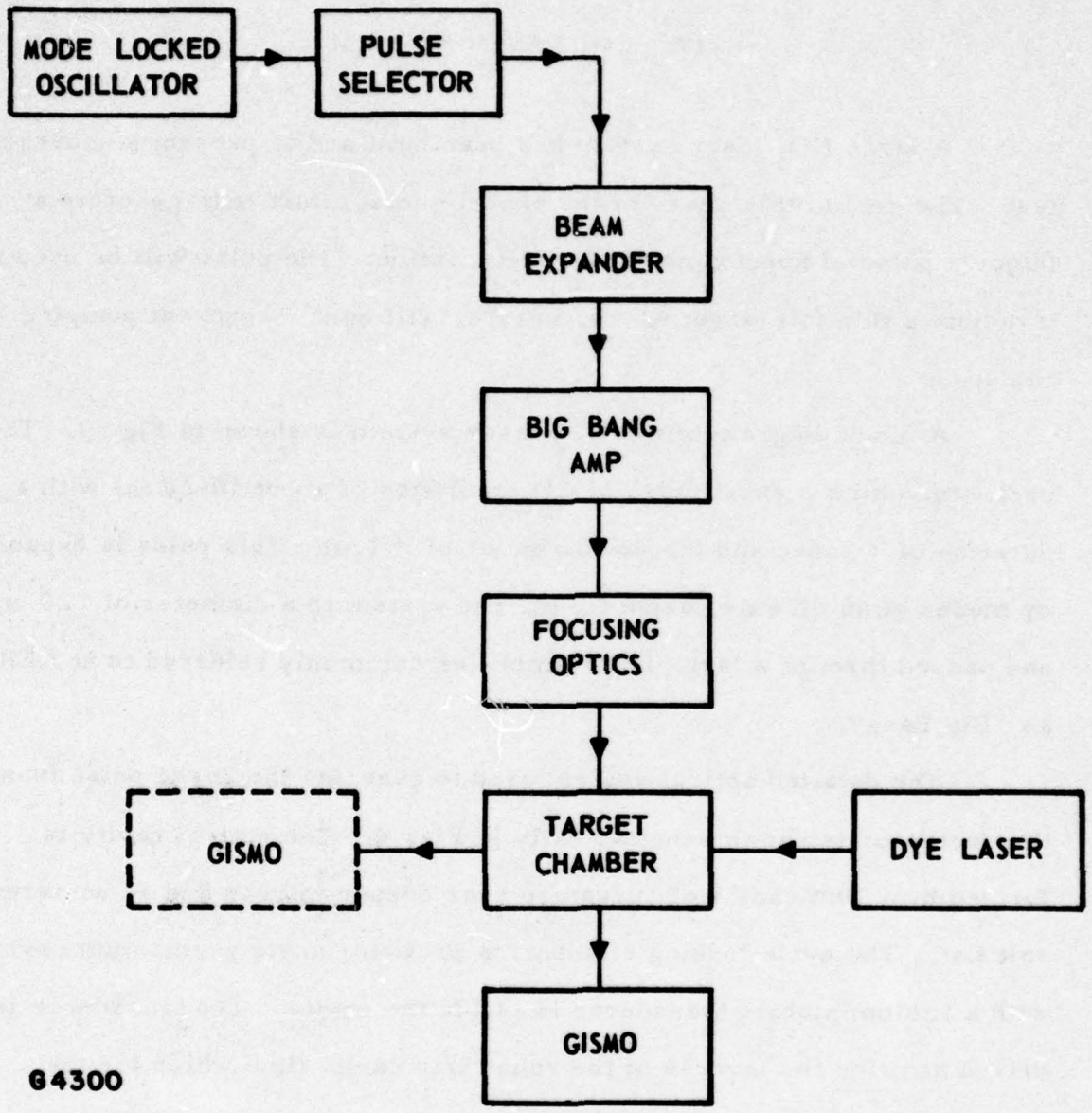

Fig. 3 Block Diagram of CO_2 Laser

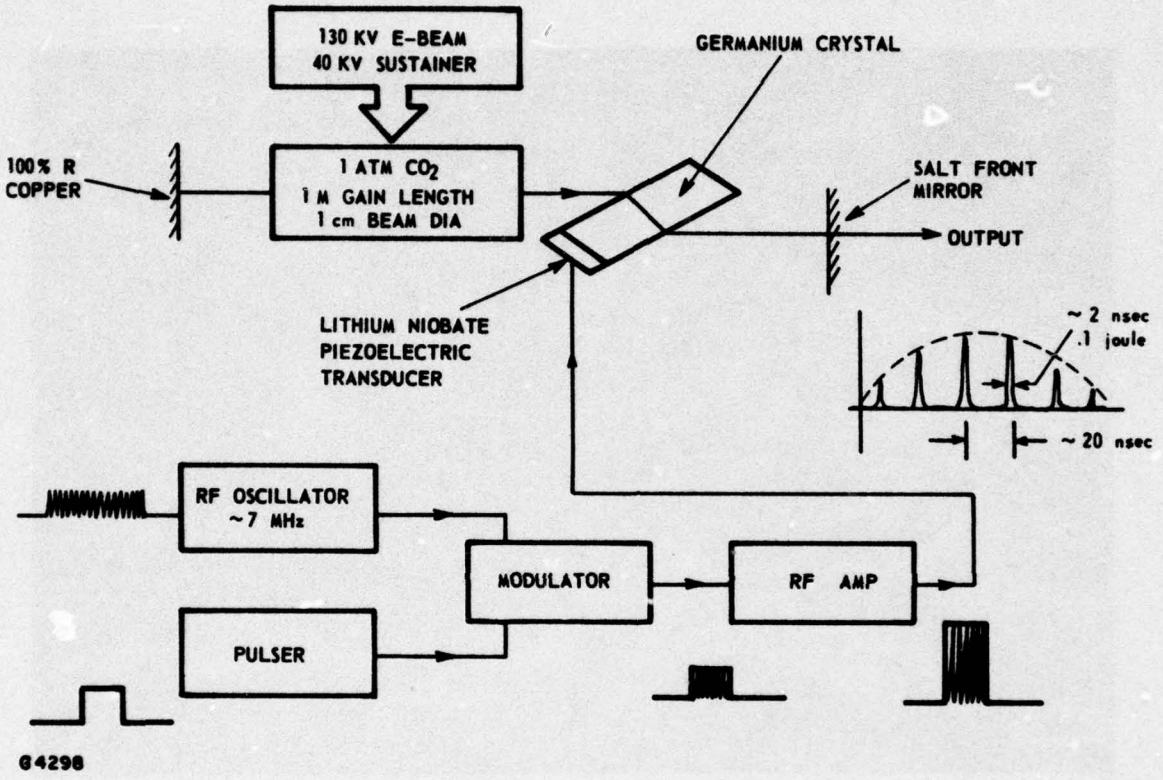

Fig. 4 Mode Locked Oscillator

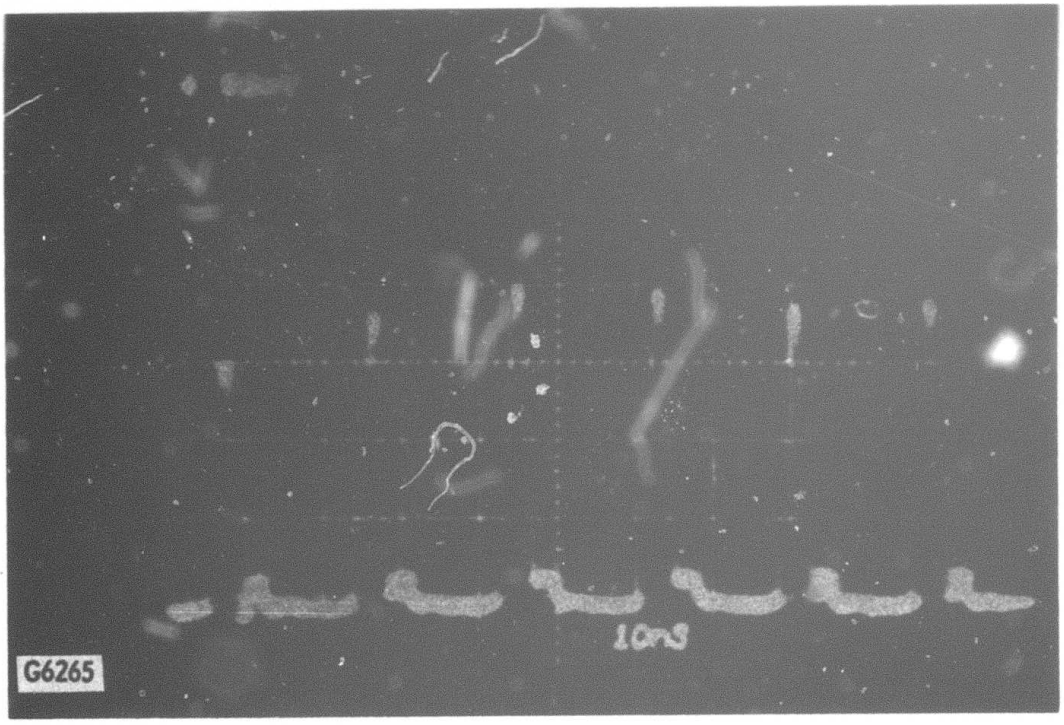

Fig. 5 Oscillograms of Mode Locked Pulse Train, 10 nsec/div

The pulse selector system consists of a Brewster angle polarizer, laser triggered spark gap and switching crystal as shown in Fig. 6. The mode locked train passes through the CdTe switching crystal at normal incidence and with no voltage applied in the ambient state. The mode locked pulse train incident on the germanium Brewster plate is polarized due to the presence of the ZnSe windows and germanium mode locking crystal which are also set at Brewster's angle. It follows that the mode locked pulse train passes through the germanium plate with no reflection and is deflected into the spark gap by a small copper mirror. The pressure and gap spacing are adjusted so that one of the early pulses in the train has sufficient energy to break down the gap. The voltage pulse switched by the spark gap as shown in Fig. 7, and time delay are determined by lengths of transmission line. With a pulse width and time delay of one-half the interpulse spacing, the voltage pulse across the CdTe switching crystal occurs at the passage of the next pulse in the train. With the gap charged to 26 kV, 13 kV appears across the crystal and polarization of the next pulse after spark gap breakdown is rotated by $\pi/2$. Approximately 80% of this pulse is reflected by the germanium plate and is diverted by the remaining mirror system to the input of beam expander. An oscillogram trace of the switched out pulse at the entrance of the beam expander is shown in Fig. 8.

After the beam is expanded to ~20 cm diameter by the off axis mirror system, the pulse is passed through Big Bang which is operated as a single pass amplifier. Calculations indicate that with 10 mj input, 50j should be obtained assuming a small signal gain-length product of 12.

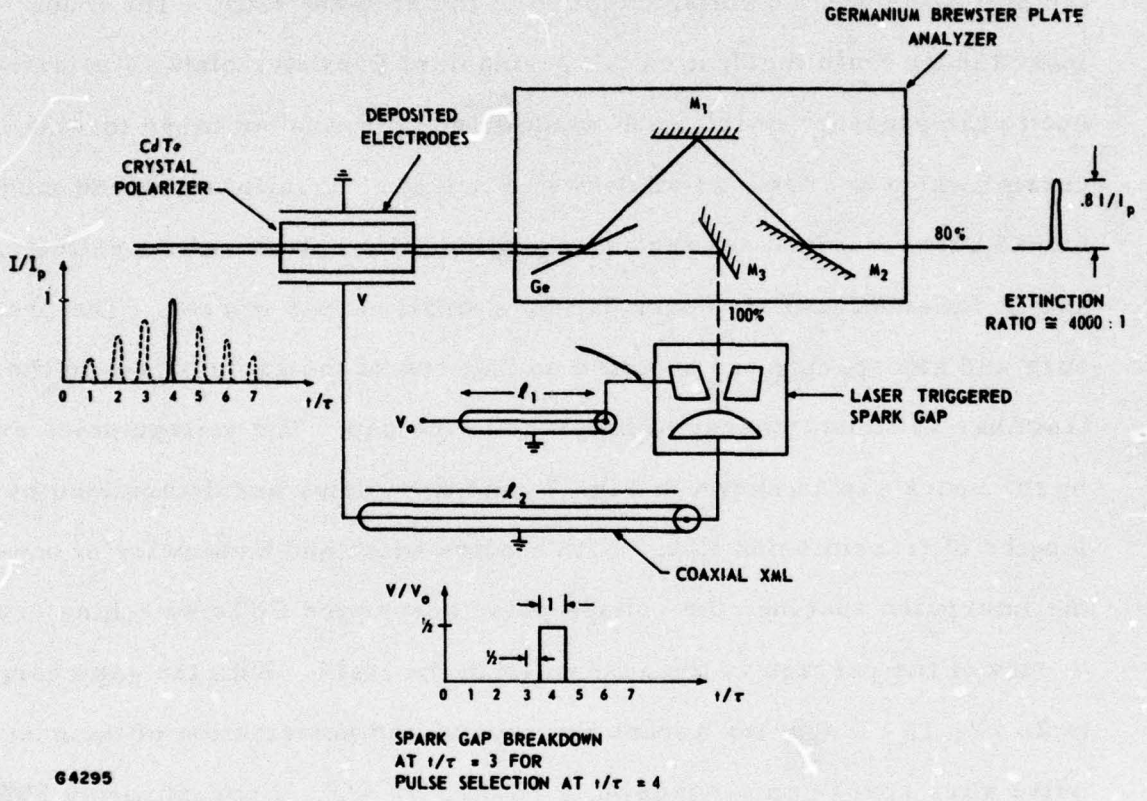

Fig. 6 Pulse Selector

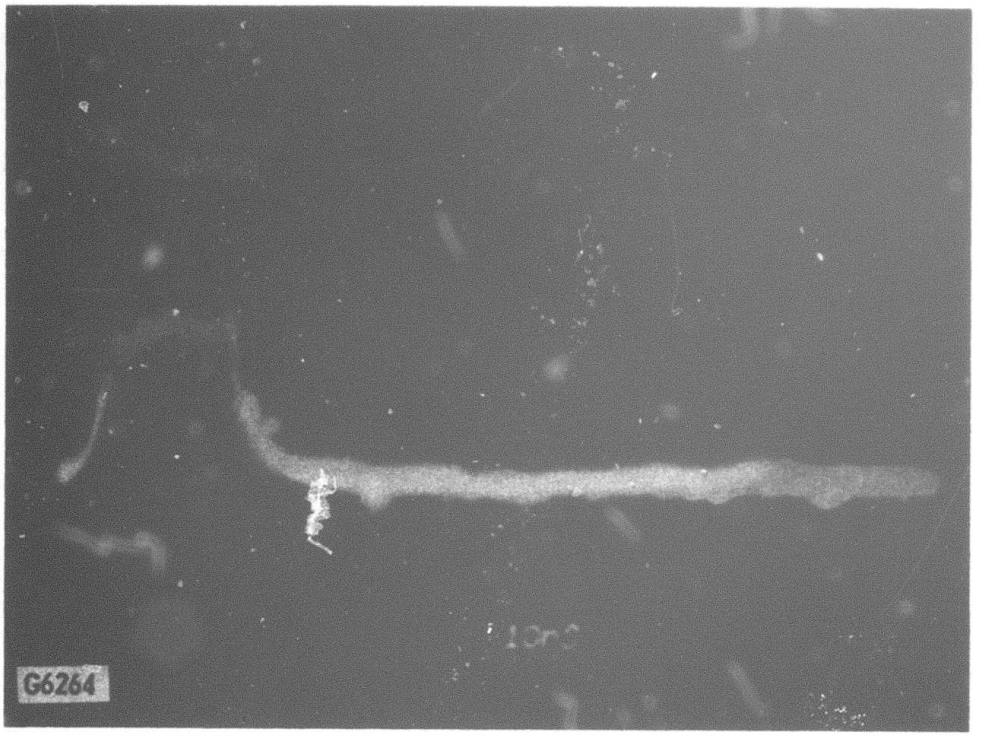

Fig. 7 Laser Triggered Spark Gap Voltage Pulse, 10 nsec/div

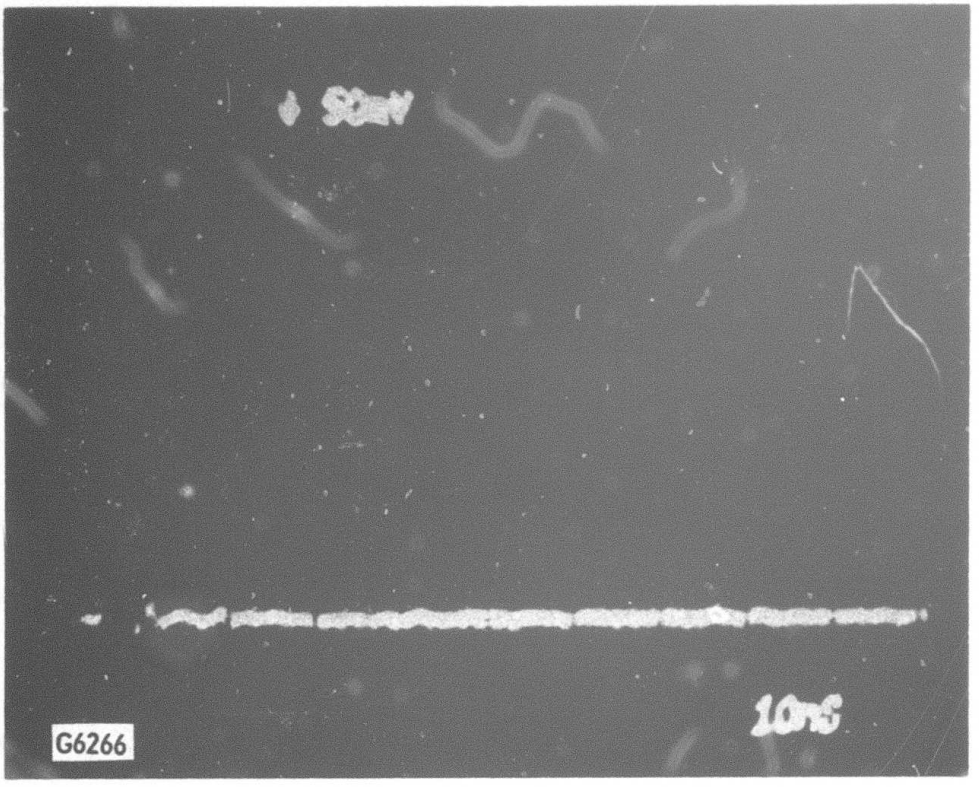

Fig. 8 Oscillogram of a Single 2 nsec, CO_2 Laser Pulse, 10 nsec/div

In previous experiments, a gain-length product of 14 was stood off without parasitic oscillation.

At the writing of this report, the switched out pulse has been amplified by Big Bang but, unfortunately, a parasitic mode was introduced by the large aperture beam expander and the exact amount of short pulse amplification is uncertain. The source of the parasitic mode is involved with the off axis beam expander. This parasitic mode can be eliminated by a change in the configuration of the optical train as confirmed by preliminary experiments. At this time we are continuing amplification experiments and expect to proceed with target experiments shortly.

V. TARGET CHAMBER

Experiments on the spectroscopy of the foil target and the lithium vapor must be conducted in vacuum because of the short extinction length of soft x-rays in air as well as CO_2 laser breakdown at atmospheric pressures. A vacuum tank was constructed to house the CO_2 laser focusing optics target foil and lithium vapor source as shown schematically in Fig. 9.

The amplified large aperture CO_2 laser beam enters the vacuum chamber through a salt window and is directed onto the focusing mirror by a turning flat. The concave mirror, 25 cm diameter and 160 cm focal length focuses the beam onto the gold foil in an off axis manner to avoid cutting a hole in the turning flat. Due to the high F-number of the system, the astigmatism of the optical system is low and near diffraction limited focusing can be maintained. As mentioned above, the salt window serves as the vacuum interface so that all focusing of the CO_2 laser beam is done under evacuated conditions to avoid air breakdown.

The actual target chamber is isolated from the rest of the optical system by a large aperture vacuum valve to permit greater experimental flexibility. Twelve target foils are mounted on a wheel which has translational and rotational control from the outside to allow focal spot positioning as well as changing of targets without bringing the entire system up to atmosphere.

Several viewing ports have been provided in the target chamber for diagnostics. The port directly opposite the foil and the one at 45°

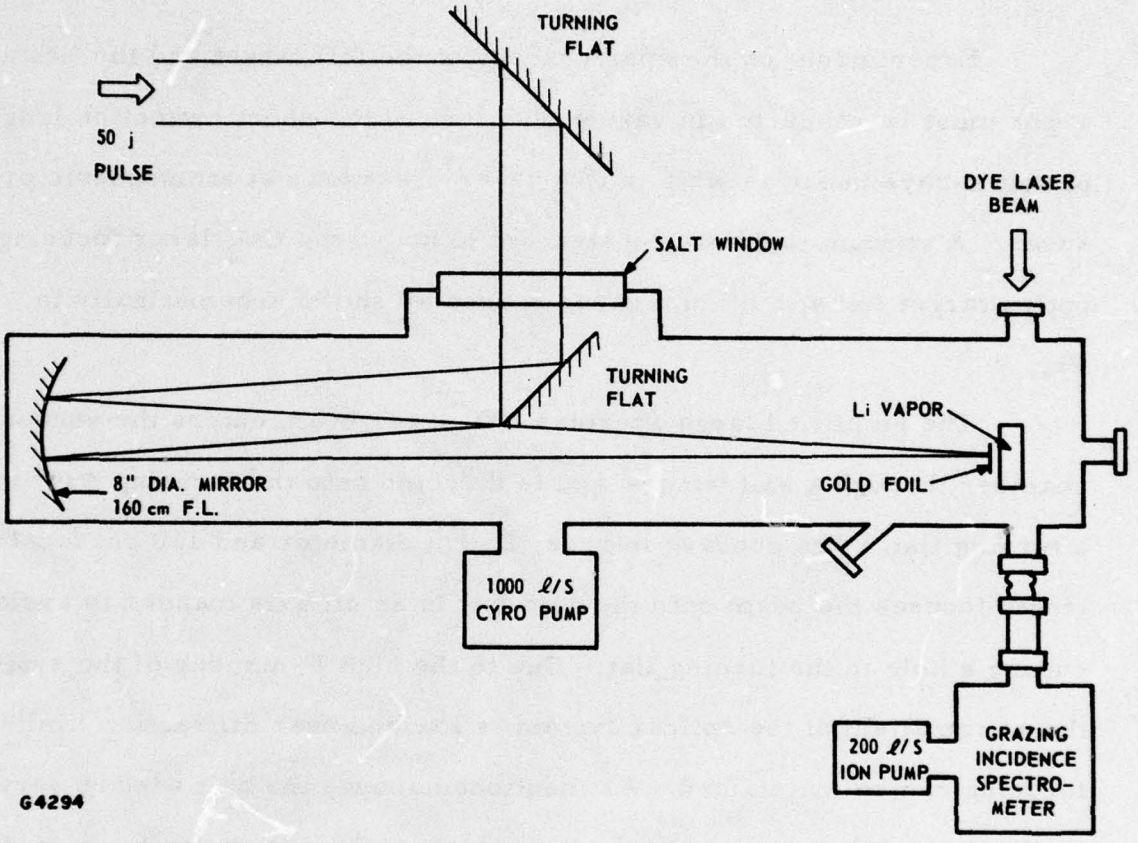

Fig. 9 Focusing Optics and Target Chamber

provide both front and rear viewing of the emission spectrum of the laser heated target foil. The transverse ports are for the dye laser input and observation of 199Å fluorescence.

The entire vacuum chamber is constructed of stainless steel with copper crush seals wherever possible. Non-greased viton seals are used elsewhere. The pumping system consists of a carbon vane roughing pump, zeolite molecular sieve intermediate pump and a 1000 ℓ/sec closed cycle helium cryogenic cold plate. These pumping systems insure oil free operation with high pumping speed. The restriction of no oil pumps, i.e., diffusion or standard mechanical roughing pumps, stems from the presence of soft x-ray fluxes which easily crack oil films leaving hard to clean carbon deposits on windows and other optical surfaces.

The vacuum interface through which the CO_2 laser beam passes is a salt window of approximately 200 cm^2 area and 2 inches in thickness. To prevent clouding due to water absorption, the window is shrouded with a slow flow of dry air and heating tapes.

VI. EXPERIMENTAL STATUS SUMMARY

The numerous subsystems which comprise the X-Ray Laser Experiment are either fully or close to completion. A single CO_2 laser pulse has been isolated from the train of mode locked pulses and expanded to fill the large aperture of the "Big Bang" amplifier. The discharge characteristics of the amplifier have been confirmed and it is ready to accept the single pulse. There are some problems associated with parasitic amplification caused by off axis feedback from the beam expander and on axis feedback from the oscillator output mirror and target chamber and experiments are underway to remove these feedback sources.

The target chamber and beam focusing optics are completely assembled and the cryo pumping system has been checked out. The target foils have been mounted, the positioning controls have been assembled, and tested under vacuum.

The grazing incidence spectrometer is fully assembled and has been vacuum checked. The ion pumping system insures no oil deposition on the grating and is compatible with the cryo pumping system of the target chamber.

The dye laser system has been built and checked and laser output has been obtained at 9584Å. The bandwidth of the grating tuned output is ~ 10Å and a telescope has been purchased to reduce the bandwidth to a few angstroms.

The experimental program for the remainder of the work period will consist of amplifying the short pulse and irradiating foil targets. The

spectrum of the foil plasma radiation will be recorded with the grazing incidence spectrometer. If time permits, the lithium vapor will be generated and dye laser absorption experiments will be performed.

APPENDIX A

OPTICAL PUMPING METHOD FOR A SOFT X-RAY LASER

by

H. A. Hyman, S. A. Mani and J. D. Daugherty

ABSTRACT

An optical pumping scheme is considered for obtaining laser action on the lithium-ion, 199 Å line. Excitation is initially stored in a highly-energetic metastable state, with an effective lifetime in the active laser medium of several nanoseconds. The required pumping power can therefore be reduced by several orders-of-magnitude, relative to techniques attempting to populate the upper laser level directly. Lasing is subsequently achieved through a stimulated, resonant Raman process, using a tunable dye laser. For an initial lithium vapor density of 10^{14} cm^{-3}, a gain ~10 cm^{-1} is predicted.

The possibility of achieving laser action on the lithium-ion, 199 Å line is considered. The present approach utilizes a two-stage, optical pumping scheme, in which excitation is initially stored in a highly-energetic, metastable state, with an effective lifetime of several nanoseconds. The intensity and risetime requirements on the pump source can thus be reduced by several orders-of-magnitude over methods which propose to populate the upper laser level directly. Lasing is subsequently achieved through a stimulated resonant Raman process,[1-3] using a tunable, infrared dye laser. Our calculations show that an initial lithium vapor density $\sim 10^{14}$ cm^{-3} is optimum, in that it allows the metastability to be preserved for several nanoseconds, while providing sufficient gain for lasing to occur in a single pass over a modest gain length (~3 cm). Although the use of metastable, helium-like ions for X-ray lasers has been suggested previously,[4, 5] neither the resonant Raman process nor the critical effect of the operating density on the degree of metastability were considered in this context. In particular, due to the fast destruction rate of the metastable state by electron collisions (see below), the feasibility of utilizing metastables is very much dependent on the details of the overall system.

A partial energy level diagram for the various ionization stages of lithium is shown in Fig. A-1. The neutral lithium atoms are initially in the $1s^2 2s$ ground state. The primary, soft X-ray pump source is anticipated to be a laser-produced plasma, and we have found that the radiation from a plasma approximating a 50 eV black body preferentially photoionizes a 1s, K-shell electron, the ratio $\langle\phi\sigma_{1s}\rangle/\langle\phi\sigma_{2s}\rangle$ being ~20, where ϕ is the black body photon flux and the brackets denote a convolution of the radiation spectrum with the appropriate cross section ($\sigma_{n\ell}$). Photoionization of the K-shell

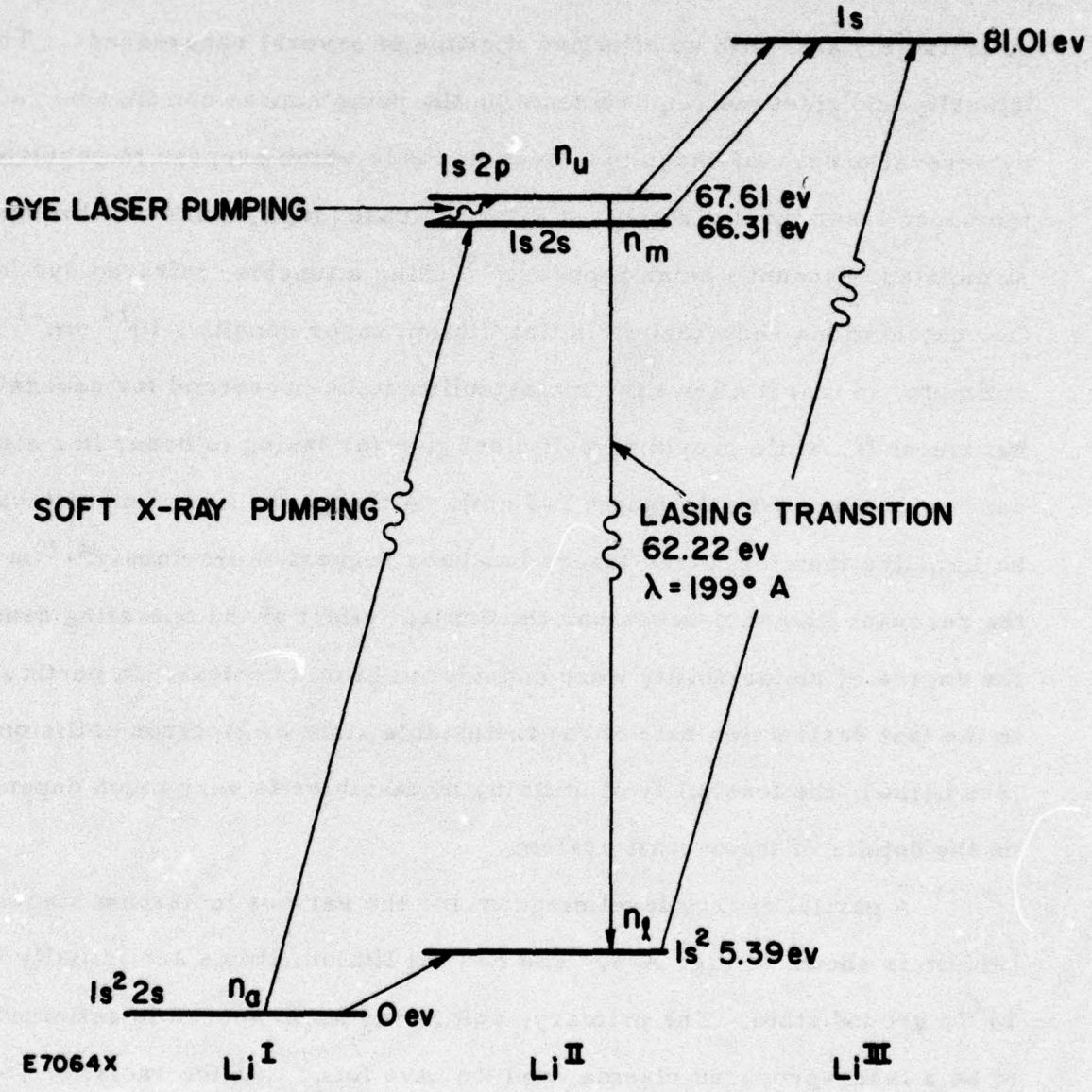

Fig. A-1 Lithium Energy Levels and Pumping Scheme

produces highly-excited ions in the $1s2s\,^{(1,3)}S$ states, with the ratio of triplets to singlets being about 3:1. For the present scheme we are concerned only with the singlet level; the triplets absorb pump flux, and therefore represent an efficiency loss, but do not otherwise affect the laser model. Since the 1s2s state lies below the next higher ionization threshold, further ionization due to the Auger effect is not possible. In addition, the 1s2s ^1S level can only decay to the $1s^2\,^1S$ ground state by two-photon emission, a process with a lifetime[6] ~500 μsec (the 1s2s ^3S lifetime is ~100 sec). The 1s2s ^1S ions are therefore metastable, so that excitation can be built up and stored over a reasonable period of time.

The dominant loss mechanism for the metastable state is mixing with the nearby 1s2p ^1P level, due to collisions with the ejected photoelectrons. The ^1P then undergoes spontaneous radiative decay in ~40 psec to the $1s^2\,^1S$ lower laser level. Radiation from a 50 eV black body produces photoelectrons with an average energy of ~25 eV, so that, assuming a Maxwellian velocity distribution, we obtain an electron impact rate[7] $\sim 3 \times 10^{-7}$ cm^3/sec, for the transition 1s2s $^1S \rightarrow$ 1s2p ^1P. Thus, for example, with an electron density of $\sim 8 \times 10^{16}$ cm^{-3}, the effective lifetime of the "metastable" state would only be 40 psec (the same as the 1s2p ^1P state), and the advantage of pumping a metastable level would clearly be lost. It is therefore not the intrinsic lifetime of the ion (~500 μsec) that determines the pumping and energy storage times, but rather the effective metastability of the ion in the active laser medium. For a reasonable photon flux, the gas is completely ionized, so that the electron density becomes approximately equal to the initial, neutral vapor density (n_{ao}). Our model indicates that $n_{ao} \approx 10^{14}$ cm^{-3} allows the metastability to be retained for several nanoseconds. To reiterate, the key point is that one has control over the degree of metastability, and in turn the pumping requirements, by properly choosing the initial operating density.

During the metastable pumping step, the rate equations describing the temporal evolution of the number densities of electrons (n_e), ground-state atoms (n_a), metastable 1s2s ions (n_m), 1s2p ions (n_u), and $1s^2$ (lower laser level) ions (n_ℓ) are given by

$$\frac{dn_e}{dt} = \langle(\sigma_{1s} + \sigma_{2s})\phi\rangle n_a + \langle\sigma_{1s'}\phi\rangle n_\ell + \langle(\sigma_{1s''} + \sigma_{2s''})\phi\rangle n_m + n_e (R_a n_a + R_m n_m + R_u n_u) \quad \text{(A-1)}$$

$$\frac{dn_a}{dt} = -\langle(\sigma_{1s} + \sigma_{2s})\phi\rangle n_a - R_a n_e n_a \quad \text{(A-2)}$$

$$\frac{dn_m}{dt} = \langle\sigma_{1s}\phi\rangle n_a - \langle(\sigma_{1s''} + \sigma_{2s''})\phi\rangle n_m - n_e (R_m n_m + R_{mu} n_m - R_{um} n_u) \quad \text{(A-3)}$$

$$\frac{dn_u}{dt} = -n_e (R_u n_u + R_{um} n_u - R_{mu} n_m) - A n_u \quad \text{(A-4)}$$

$$\frac{dn_\ell}{dt} = \langle\sigma_{2s}\phi\rangle n_a + R_a n_e n_a + A n_u - \langle\sigma_{1s'}\phi\rangle n_\ell \quad \text{(A-5)}$$

In the above, R_a, R_m and R_u are the electron-impact ionization rates[8] of neutral atoms, 1s2s and 1s2p states, respectively; R_{mu} and R_{um} are the electron-impact mixing rates for the transitions $1s2s \rightleftarrows 1s2p$; A is the spontaneous decay rate of the 1s2p level; $\sigma_{n\ell}$ is again the photoionization cross section[9] for the $n\ell$ th electron; and ϕ is the photon flux.

Although the 50 eV black-body radiation preferentially photoionizes the K-shell of the neutral lithium, we have found it to be advantageous to further tailor the spectrum. A thin foil (~1000 Å - 2000 Å) of beryllium

turns out to be an ideal filter, having an L-edge at 9.3 eV and a K-edge at 108 eV. The ratio $\langle\phi\sigma_{1s}\rangle/\langle\phi\sigma_{2s}\rangle$ is thus enhanced, but more importantly the photon flux capable of photoionizing the metastable 1s2s state is significantly reduced. Figure A-2 shows the flux (in photons/cm^2-eV-sec) from a 50 eV black body, with no filter (dashed curve) and with a 1000 Å thick Be filter (solid curve). The depletion of flux near the Li^+ (1s2s) L-edge (at ~15 eV) and K-edge (at ~107 eV) is evident. Additional filtering of the spectrum may prove to be useful, and we are currently considering this possibility.

The rate Eqs. (A-1)-(A-5) have been solved numerically,[10] using the filtered radiation spectrum shown in Fig. A-2 and taking a 3 nsec, trapezoidal pulse, which is assumed to rise linearly for 1 nsec, remain constant for 1 nsec, and decay linearly for 1 nsec. Figure A-3 shows a typical computer solution for the densities (normalized to the initial vapor density, n_{ao}) as functions of time, with the solid curve representing the metastable (1s2s ^{1}S) density and the dashed curve representing the lower laser level (1s^2 ^{1}S) density. The case shown corresponds to the conditions $n_{ao} = 10^{14}$ cm^{-3} and $\langle\phi\sigma_{1s}\rangle = 8.6 \times 10^8$ sec^{-1}, which in turn corresponds to an incoherent pump intensity $I = 2.5 \times 10^9$ W/cm^2 of 66 eV photons and a photoionization cross section[9] at threshold of 3.6×10^{-18} cm^2. It is apparent from the figure that there is a significant inversion between the metastable and ground states. At the end of the soft X-ray pump pulse (after 3 nsec), the inversion slowly decays due to the electron mixing process described earlier.

Once the metastable density has been built up, an infrared dye laser tuned to the λ = 9584.1 Å, 1s2s ^{1}S → 1s2p ^{1}P transition[11] is switched on. Lasing at 199 Å occurs in a stimulated resonant Raman (SRR), anti-Stokes process. It should be noted that for the SRR process an inversion is required between the metastable level and the ground state, but not necessarily between the intermediate ^{1}P level and the ground state. The

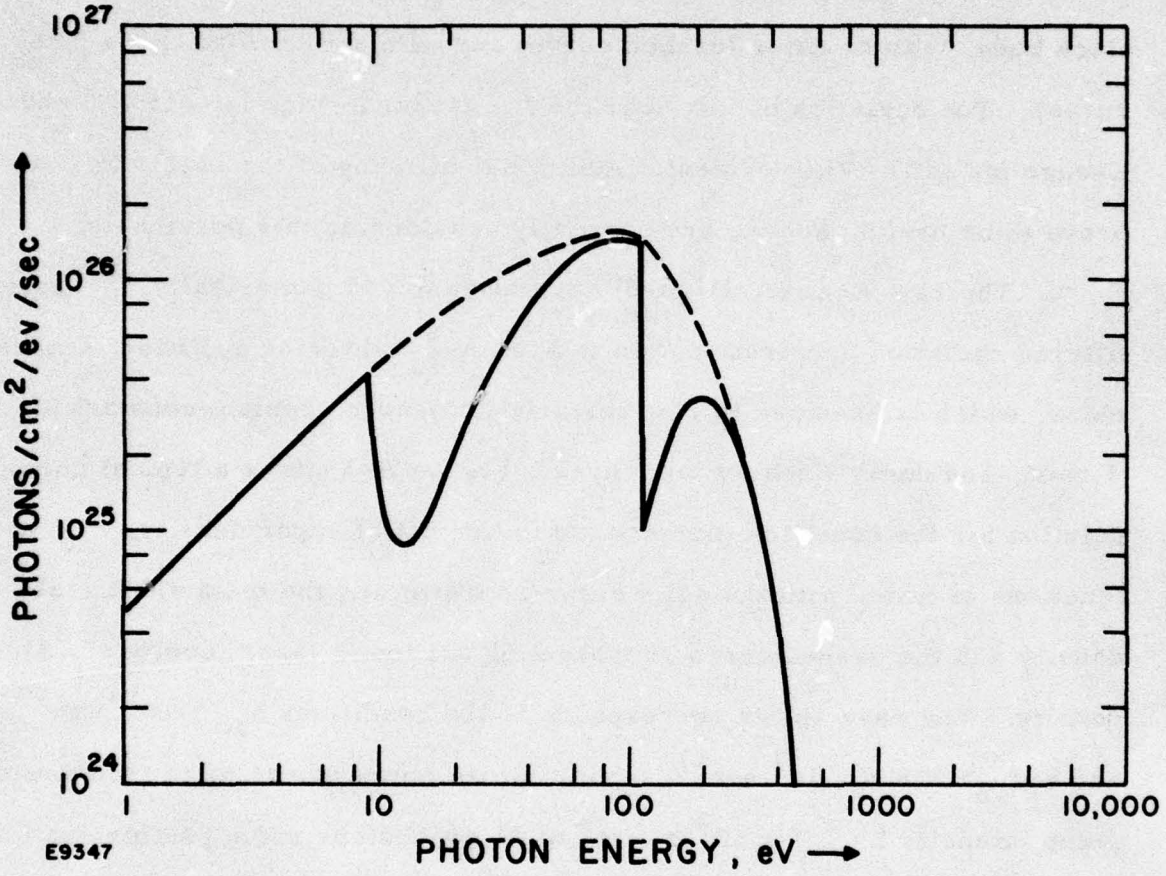

Fig. A-2 Emission Spectrum from a 50 e V Black Body, with no Filter (Dashed Curve) and with a 1000 Å Thick Be Filter (Solid Curve)

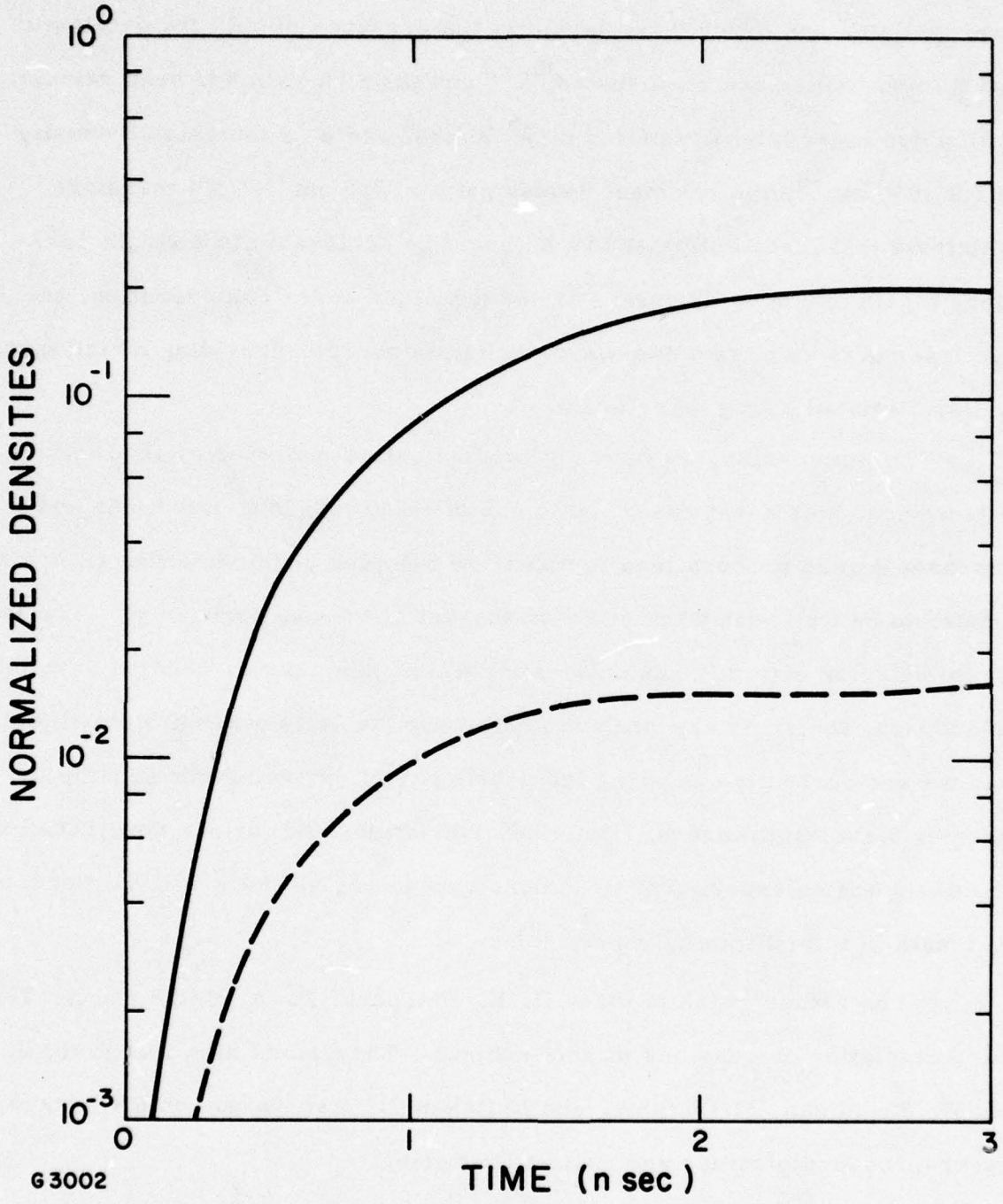

Fig. A-3 $1s2s\ ^1S$ Metastable (Solid Curve) and $1s^2\ ^1S$ Lower Laser Level (Dashed Curve) Densities (Normalized to the Initial Lithium Vapor Density, n_{ao}) vs Time

quantum-mechanical, time-dependent amplitude equations for the metastable, intermediate, and lower laser levels in the presence of both the dye laser and Raman fields have been solved,[3, 10] and the SRR gain has been calculated. With a dye laser intensity of 1.5×10^5 W/cm^2 and a ^1S metastable density of 2×10^{13} cm^{-3}, the resonant Raman gain is ~10 cm^{-1}. We therefore anticipate that laser action at 199 Å should be achievable in a single pass along a gain length of ~3 cm. For the technique under consideration, the dye laser acts as a traveling-wave excitation source, providing a collinear, well-collimated X-ray laser beam.

To summarize, we have outlined an optical pumping method for a lithium-ion, soft X-ray laser. The use of relatively long-lived ions and the resonant Raman process lead to moderate pumping requirements, all of which appear to be well within the state-of-the-art of present technology. The laser would be volumetrically scalable as increased pump power becomes available. In addition, the same approach should be applicable to other lithium-like ions, and we are currently exploring the possibility of extending our scheme to shorter-wavelength lasers. Detailed calculations and further considerations for designing an experiment to demonstrate lasing at 199 Å will be discussed at length in a forthcoming paper.[10]

The authors wish to thank H. E. Petschek, H. A. Bethe and E. Teller for stimulating discussions on this subject. They would also like to thank H. W. Friedman, M. Sirchis, and I. Itzkan for discussions on dye lasers, laser-produced plasmas and Raman scattering.

REFERENCES

1. I. M. Beterov, Yu. A. Matyugin, and V. P. Chebotaev, Zh. Eksp. Teor. Fiz. 64, 1495 (1973), [Sov. Phys. - JETP 37, 756 (1973)].

2. E. V. Baklanov, I. M. Beterov, B. Ya. Dubetskii, and V. P. Chebotaev, Pis'ma Zh. Eksp. Teor. Fiz. 22, 289 (1975) [Sov. Phys. - JETP Letters 22, 134 (1975)].

3. S. A. Mani (to be published).

4. H. Mahr and U. Roeder, Opt. Commun. 10, 227 (1974).

5. A. A. Vekhov, V. N. Makhov, F. A. Nikolaev, and V. B. Rozanov, Kvant. Electron (Mosc.) 2, 1318 (1957), [Sov. J. Quant. Electron. 5, 718 (1975)].

6. G. W. F. Drake, G. A. Victor, and A. Dalgarno, Phys. Rev. 180, 25 (1969).

7. C. W. Allen, Astrophysical Quantities (Athlone Press, 3rd Ed., London, England, 1973).

8. W. Lotz, Inst. für Plasma Physik, Garching, Germany, Rept. IPP 1/62, May (1967).

9. W. D. Barfield, G. D. Koontz, and W. F. Heubner, JQSRT 12, 1409 (1972).

10. S. A. Mani, H. A. Hyman, and J. D. Daugherty (to be published).

11. Y. Accad, C. L. Pekeris, and B. Schiff, Phys. Rev. A4, 516 (1971).

APPENDIX B

EFFECT OF AUTOIONIZING STATES ON THE LITHIUM SOFT X-RAY LASER

by

H. A. Hyman and S. A. Mani

ABSTRACT

The effects of autoionizing states on the lithium-ion 199 Å laser are considered. A general treatment of the problem is developed, and results of detailed modeling calculations are given.

1. INTRODUCTION

The possibility of achieving laser action on the lithium-ion 199 Å resonance line has been considered in detail in a previous paper[1]. Very briefly, the concept is as follows: 50 eV blackbody radiation from a CO_2 laser-produced plasma preferentially photoionizes a K-shell electron of neutral lithium, producing ions in the $1s2s\,^{1,3}S$ metastable states. For an initial lithium vapor density $\lesssim 3 \times 10^{14}$ cm^{-3}, it was found that the collision processes involving the free photoelectrons are slow enough to allow the inversion between the metastables and the $1s^2$ lithium-ion ground state to build up over a period of several nanoseconds. After a sufficient accumulation of metastables, a short pulse dye laser, tuned to the 9584.1 Å, $1s2s\,^1S \rightarrow 1s2p\,^1P$ transition, is turned on, and lasing at 199 Å occurs due to a stimulated resonant Raman anti-stokes process. It was also pointed out that resonant Raman pumping from the $1s2s\,^3S$ state should be possible, using a dye laser tuned to the $1s2s\,^3S \rightarrow 1s2p\,^1P$ transition at 3879.8 Å. Due to the very small dipole moment[2] for this transition, $\approx 2.8 \times 10^{-21}$ esu, a considerably greater Raman pump intensity is required compared to the $^1S \rightarrow {}^1P$ process. Nevertheless, the use of the triplet metastables appears feasible and the results of modeling calculations for the triplet inversion density are presented in Section 3. A more complete description of the scheme outlined above can be found in Ref. 1.

In our earlier work[1], we neglected the presence of autoionizing levels, which typically give rise to several series of narrow resonances superimposed on the photoionization continuum. Including autoionization effects in our existing model, leads to a marked reduction in the inversion density, and in fact, such effects are expected to be of importance for virtually all

X-ray laser schemes involving photoionization of inner-shell electrons. The present paper therefore discusses a modification of the original lithium-ion laser scheme, which manages to circumvent most of the problems associated with the autoionizing states. Although our results are applied specifically to the lithium case, the treatment is sufficiently general so as to be applicable to a wide class of photoionization-pumped X-ray lasers.

2. AUTOIONIZING STATES

In view of the lack of specific data for the spectra of interest, and in order to develop a general treatment of the problem, we will use the well-known Fano-Cooper theory [3,4] of autoionization, and their definitions and terminology will be used here without further explanation. The case under consideration corresponds to [4] "full participation of the outer electron", and the important matrix elements are thus dependent primarily on the spatial part of the wavefunction near the nucleus (i.e. at small radial distances). It can then be shown [4] that the decay width of the nth member of a Rydberg series of autoionizing levels can be written as $\Gamma_n \approx N_n^2 \bar{\Gamma}$, where N_n is a normalization factor ($N_n^2 \sim 1/n^{*3}$, with n^* the effective quantum number) and where $\bar{\Gamma}$ is called the reduced width and is independent of n. Similarly, for the photoexcitation of an inner-shell electron to the nth state, we can write $f_n \approx N_n^2 \bar{f}$ where $\bar{f}$ is the reduced oscillator strength. Finally, we note that the absorption cross section at the center of the nth line Q_n^o, and the corresponding optical depth τ_n^o, are proportional to the quantity $f_n/\Gamma_n \approx \bar{f}/\bar{\Gamma}$. We can therefore take $Q_n^o \approx \overline{Q^o}$ and $\tau_n^o \approx \overline{\tau^o}$, where we have introduced the reduced cross section and optical depth which

are again constants characterizing the complete series.

The rate of photoexcitation to all the states of a Rydberg series of autoionizing levels, due to a blackbody, or similar broadband pump flux, ϕ, is given by

$$R_A = \sum_n \int \phi(\nu)\, Q_n(\nu)\, d\nu \approx \tilde{\phi} \sum_n \int Q_n(\nu)\, d\nu$$

$$= \tilde{\phi} \left(\frac{\pi e^2}{mc}\right) \sum_n f_n \qquad \text{(B-1)}$$

Taking $\phi(\nu)$ outside both the integral and the summation, and replacing it by a mean flux, $\tilde{\phi}$, is justified by the fact that the blackbody flux does not vary much over the energy range spanned by the important (i.e., first few) members of the series. We also assume throughout the paper that the cross section $Q_n(\nu)$, has the standard Lorentz resonance shape, which is appropriate for large values of q, the line profile parameter [3,4]; this is a very good approximation for the cases of interest. With $\tilde{\phi}$ in units of photons/cm^2 - eV - sec, the rate can be written as

$$R_A = 1.1 \times 10^{-16}\, \tilde{\phi} \sum_n f_n \ (\text{sec}^{-1}) \qquad \text{(B-1a)}$$

We now wish to consider more specifically the spectra of neutral and singly-ionized lithium. Three series of autoionizing states are of primary interest. (i) <u>Li ($1s^2 2s\ ^2S$) → Li [($1s2s\ ^3S$) $np\ ^2P$]:</u> A prominent series in neutral lithium is expected to arise from the excitation of a K-shell electron to quasi-bound p-states, converging on the $1s2s\ ^3S$ threshold (see Fig. B-1), and indeed this series has been observed by

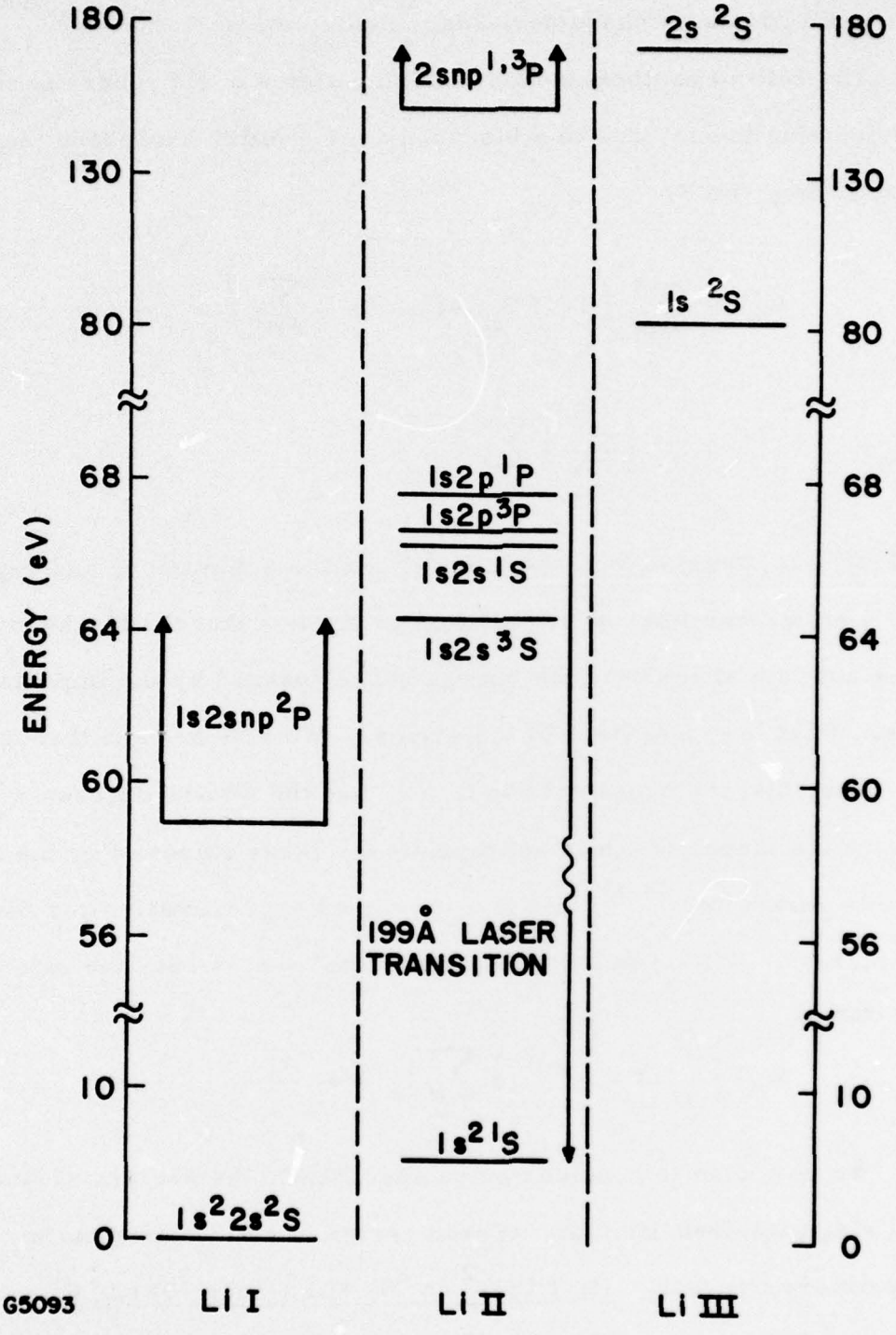

Fig. B-1 Lithium Energy Level Diagram (Note Changes in Energy Scale)

Ederer, et al[5]. Since there is only the single $1s^2\epsilon p\ ^2P$ adjacent continuum, all of the $(1s2s\ ^3S)\,np\ ^2P$ states rapidly decay to the Li II($1s^2$) lower laser level. The first member of the series is at 58.91 eV and has a width[6, 7] $\Gamma = .007$ eV. While no data exists in the literature on the oscillator strength, unpublished results[8] suggest $f \approx .25$. The absorption cross section at the center of the line is then

$$\overline{Q^o} = \frac{2r_e f}{\Gamma(cm^{-1})} = 2.5 \times 10^{-15}\ cm^2 \qquad (B\text{-}2)$$

where r_e is the classical electron radius ($r_e = 2.82 \times 10^{-13}$ cm). For the remainder of the series, we use the approximate relation $f_n \sim 1/n^{*3}$, together with the n^* values given in Ref. 5, to obtain $\sum f_n \approx .36$. Thus knowing the flux from the 50 eV blackbody, we can use formula (B-1a) to calculate the total rate for filling the $1s^2$ lower laser level due to excitation and subsequent autoionization of the $(1s2s\ ^3S)\ np\ ^2P$ series. It is of interest to compare this rate to that for producing the $1s2s\ ^1S$ upper laser level by direct photoionization of the K-shell[1]; the ratio is $R_A/R\ (1s2s\ ^1S) \approx .8$, which explains the large reduction in the inversion density when this effect is included in the existing model.

There are also several series of autoionizing states converging to higher ionization thresholds. The first such state[5] is at 60.396 eV and is nominally the lowest member of the $(1s2s\ ^1S)\ np\ ^2P$ series. The oscillator strength for this level is estimated[8] to be $\sim .005$ and is therefore negligible. The remaining levels of the various series

lie above the 1s2s ^{3}S threshold, where the situation is complicated by the presence of several adjacent continua. Above the ^{3}S limit, autoionization directly into excited states of the ion should be favored, leading to a possible enhancement of the inversion density. However, such effects are expected to be of relatively minor importance and have not been included in the model.

(ii) $\underline{Li^+ (1s2s\ ^1S) \rightarrow Li^+ (2snp\ ^1P)}$: The 2snp ^{1}P states autoionize to the Li III (1s) level, and therefore represent a loss mechanism for the 1s2s ^{1}S upper laser level, which must be added to the destruction rate due to direct photoionization of both the 1s and 2s electrons, plus the small collision-induced losses. Our modeling calculations indicate that such autoionization effects in the Li II spectrum are much less important than those occuring in the Li I spectrum [see part (i)].

As indicated in Fig. B-1, the 2s2p ^{1}P level is at approximately 156 eV above the Li I ground state, and the series converges to the Li III (2s) threshold. From the calculations of Drake and Dalgarno[9], $\Gamma(2s2p\ ^1P) = .06$ eV. No information exists on the relevant oscillator strengths; we have therefore used f-values for the analogous helium configurations, which should be a fairly good approximation. Unfortunately, even the various helium results [10-12] are not in particularly good agreement, and so we have simply averaged the values given in Refs.(10-12). We thereby obtain $f_2 \approx .27$ and $\sum f_n \approx .35$. Using expression (B-2), we find $\overline{Q^o}$ (singlet) $\approx 3.2 \times 10^{-16}$ cm^2.

(iii) $\underline{Li^+ (1s2s\ ^3S) \rightarrow Li^+ (2snp\ ^3P)}$: The 2snp ^{3}P states are exactly analgous to the singlet series discussed above. They again autoionize to the Li III (1s) level, and thus represent a loss process for the triplet

metastable ions. The width is [9] $\Gamma(2s2p\ ^3P) = .01$ eV, and again using an average of the various helium values [10, 11, 13], $f_2 \approx .3$ and $\sum f_n \approx .36$. The absorption cross section at line center is $\overline{Q^o}$ (triplet) $\approx 2.1 \times 10^{-15}$ cm^2, which is a factor of 6.6 larger than for the singlet series, due primarily to the much smaller width.

3. MODELING CALCULATIONS

In order to contend with the autoionization effects, we have modified the original scheme somewhat, and the relevant calculations are discussed in this section. We first consider excitation of the $(1s2s\ ^3S)np\ ^2P$ series in neutral lithium, which is the most important of the various autoionization processes. From expression (B-2) we have $\overline{Q^o} = 2.5 \times 10^{-15}$ cm^2 for the lines, whereas the peak photoionization cross section is [1, 14] $Q(1s^22s \rightarrow 1s2s) \sim 4 \times 10^{-18}$ cm^2. It should therefore be possible to set up a filtering zone of lithium vapor between the pump source and the laser region with a density chosen so that the gas is optically thick in the lines and thin relative to photoionization. This can be accomplished by using either a continuous density gradient or two separate regions at different densities. The latter has been chosen for modeling purposes, and a schematic of a possible laser geometry is shown in Fig. B-2. The only difference between the earlier scheme (see Fig. 7 of Ref. 1) and the present modification is the insertion of the lithium filter region. As before, the high-power CO_2 laser beam is focused onto a foil of high-Z material, creating a thin ribbon (of width $r_o \sim 200\mu$) of hot dense plasma. The blackbody radiation from the plasma then passes through the lithium filter region, through a thin beryllium foil to further tailor the spectrum[1], and into the low-density

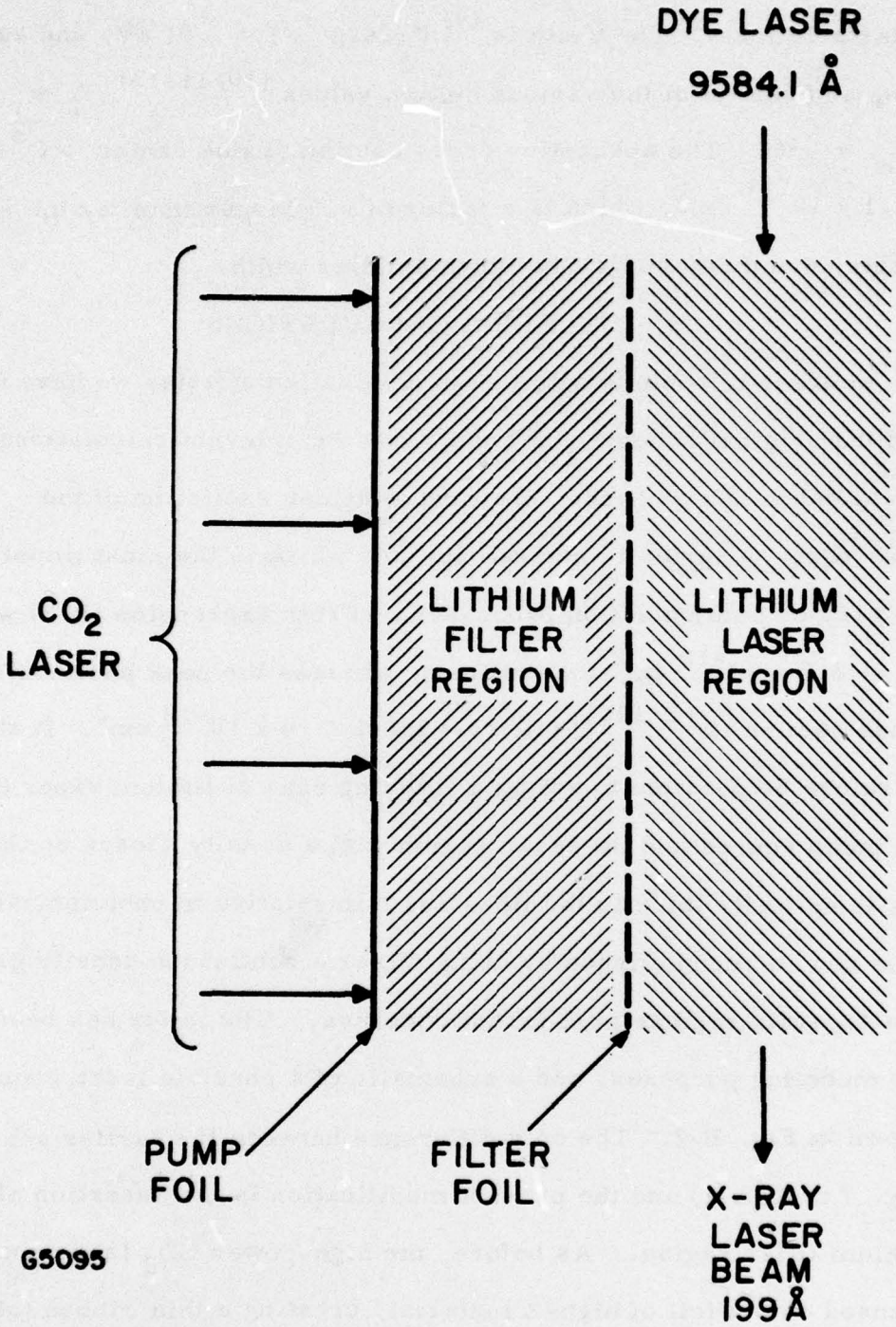

Fig. B-2 Schematic of Lithium-Ion, Soft X-ray Laser

laser region, where the lithium vapor is pumped into the Li^+ ($1s2s\ ^{1,3}S$) metastable states. The dye laser, which pumps the stimulated resonant Raman (SRR) transition, is then switched on and acts as a traveling-wave source for the 199 Å, soft X-ray laser beam. Due to the r^{-1} fall-off of the blackbody flux away from the linear plasma source, the effective transverse pumping range is limited to ~1 cm; we have therefore taken the width of the filter region and of the laser region to .5 cm each.

If the width of the filter region is denoted by Δr, then the optical depth for one line of the ($1s2s\ ^3S$) $np\ ^2P$ series can be written as

$$\tau_n(\nu, t) = Q_n(\nu) \int_{r_o}^{r_o + \Delta r} n_a(r, t)\, dr \tag{B-3}$$

where $n_a(r, t)$ is the spatially- and time-dependent ground-state lithium density. The excitation rate, after filtering, for all lines of the series is then given by

$$\tilde{R}_A \approx \tilde{\phi} \sum_n \int Q_n(\nu)\, e^{-\tau_n(\nu, t)}\, d\nu = R_A\, e^{-\overline{\tau^o}/2}\, I_o\left(\frac{\overline{\tau^o}}{2}\right) \tag{B-4}$$

with

$$\overline{\tau^o} = \overline{Q^o} \int_{r_o}^{r_o + \Delta r} n_a(r, t)\, dr \tag{B-5}$$

where R_A is the unfiltered rate, given by formula (1a), and $I_o(\overline{\tau^o}/2)$ is the modified Bessel function of order zero. The integral in expression (B-4) was evaluated using the standard Lorentz form for the

absorption cross section:

$$Q_n(\nu) = \frac{Q_n^o}{1 + |2(\nu - \nu_n)/\Gamma_n|^2} \qquad \text{(B-6)}$$

Note that the rate is now time-dependent due to the time dependence of the density, n_a. From (4), $\tilde{R}_A/R_A \sim 1/\sqrt{\overline{\tau^o}}$ for large values of $\overline{\tau^o}$, and the filter clearly becomes more effective with increased pump power and correspondingly increased transverse pumping range.

As the lithium filter evolves in time, the density of neutral atoms, n_a, falls, while the density of $1s2s\ ^{1,3}S$ metastables builds up. The blackbody flux is therefore also filtered at the positions of the $1s2s\ ^{1,3}S \rightarrow 2snp\ ^{1,3}P$ lines, thus reducing the destruction rate of metastables due to excitation of the $2snp\ ^{1,3}P$ autoionizing states. Expressions (B-4) and (B-5) can again be used to calculate the rates, but with $n_a(r,t)$ replaced by the appropriate metastable density. The fact that $\overline{Q^o}$ (triplet) / $\overline{Q^o}$ (singlet) = 6.6 makes the filter more effective for the triplets than for the singlet ions.

We have modeled the scheme shown in Fig. B-2 by numerically solving the rate equations for the number densities of electrons, neutral ground-state atoms, and lithium ions in the states: $1s2s\ ^1S$, $1s2p\ ^1P$, $1s2s\ ^3S$, $1s2p\ ^3P$, and $1s^2\ ^1S$. The rate equations are essentially the same as those given in Ref. 1, supplemented by terms for the autoionization processes. The optimum initial vapor density for the .5 cm-wide filter region was found to be 2×10^{16} cm^{-3}. For this density, the optical depth at line center for time t = 0 is $\overline{\tau^o} = 25$ and $\tilde{R}_A/R_A \approx .11$, so that we now have $\tilde{R}_A/R\ (1s2s\ ^1S) \approx .09$, a large reduction over the

value obtained earlier. Although it is tempting to simply increase the density and thereby further decrease R_A, there is a trade-off, since the larger the density, the faster is the disappearance of neutral atoms due to ionizing collisions with photoelectrons. The initial density in the laser region was taken to be $n_{ao} = 3 \times 10^{14}$ cm^{-3}, and the 50 eV blackbody pump flux was assumed to be triangular in shape, with a total duration of 2 nsec (FWHM = 1 nsec). The resulting computer solutions for the normalized inversion densities as functions of time are shown in Fig. B-3. The dashed curve is for the singlet case and represents the quantity $[n(1s2s\ ^1S) - n(1s^2)]\ /n_{ao}$, while the solid curve is for the triplets and is $[n\ (1s2s\ ^3S) - 3n(1s^2)]/n_{ao}$. The maximum singlet inversion density is 1.2×10^{13} cm^{-3}. In the previous calculation [1] of the SRR cross section, the averaging over the orientation of the atom with respect to the pump and Raman fields was omitted, this results in a factor of 3 reduction in the cross section. In addition, the effects of Doppler broadening have been incorporated into the theory [15], leading to the revised value $Q_{SRR} = 1.0 \times 10^{-13}$ cm^2 for a dye laser intensity of $\sim 10^5$ watts/cm^2. For the present example, the small signal gain for the $1s2s\ ^1S$ metastables is therefore $g_o = 1.2$ cm^{-1}. The Raman calculation for the triplets proceeds somewhat differently than for the singlet case, and a detailed theory for Raman pumping of the 199 Å line from the triplet metastables is currently being completed [15].

4. CONCLUSION

To summarize, we have reconsidered the lithium soft X-ray laser [1], taking into account previously-neglected autoionization effects. To deal with the autoionization problem, we have proposed

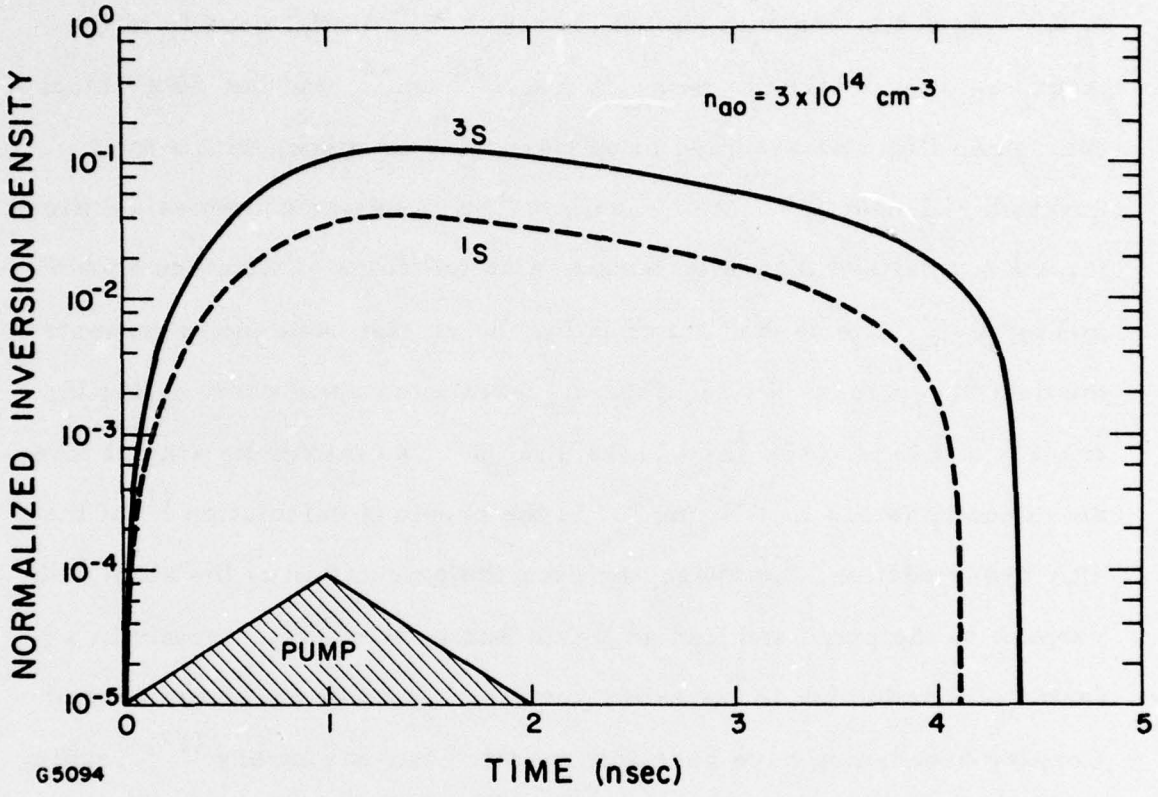

Fig. B-3 Normalized Inversion Densities vs Time: Dashed Curve is for 1s2s ^{1}S State and Solid Curve is for 1s2s ^{3}S State. The initial density in the lithium laser region was taken to be $n_{ao} = 3 \times 10^{14}$ cm^{-3}, and a triangular 2 nsec pump pulse was used in the calculation.

the use of a filtering zone of lithium vapor between the pump source and the low-density laser region. Modeling calculations have been carried out for a specific case of interest; using the revised resonant Raman cross section, a gain of 1.2 cm^{-1} is predicted. Further refinement of the model is largely contingent upon the availability of more data on photoexcitation processes in neutral and singly-ionized lithium in the soft X-ray range.

ACKNOWLEDGMENTS

The authors wish to thank D.L. Ederer, T.S. Axelrod and J.D. Daugherty for several helpful discussions.

REFERENCES

1. S.A. Mani, H.A.Hyman and J.D.Daugherty, J.Appl. Phys. 47, 3099 (1976).
2. G.W.F. Drake and A.Dalgarno, Astrophys.J. 157, 459 (1969).
3. U.Fano, Phys. Rev. 124,1866 (1961).
4. U.Fano and J.W. Cooper, Phys. Rev. 137, A 1364 (1965).
5. D.L. Ederer, T.Lucatorto and R.P. Madden, Phys. Rev. Letters 25, 1537 (1970).
6. I.R. Barden, C. Bottcher and K.R. Schneider, J.Phys. B8, L1 (1975).
7. A.H. Bhatia and A.Temkin, Phys. Rev. A13, 2322 (1976).
8. D.L. Ederer (private communication).
9. G.W.F. Drake and A. Dalgarno, Proc. Roy.Soc. London A320, 549 (1971).
10. A. Dalgarno and A.E. Kingston, Proc. Phys. Soc. 72, 1053 (1958).
11. K.S. Suh and M.H. Zaidi, Proc. Roy. Soc. A291, 94 (1966).
12. H.O. Dickinson and M.R.H. Rudge, J. Phys. B3, 1284 (1970).
13. H.O. Knox and M.R.H. Rudge, J. Phys. B2, 521 (1969).
14. W.D. Barfield, G.D. Koontz and W.F. Heubner, JQSRT 12, 1409 (1972).
15. S.A. Mani (to be published). A preliminary report on the Raman calculations is given in Avco Everett Research Laboratory Report RR431 (1976).